Single Molecule Fluorescence Microscopy Notes

Talon Chandler

February 10, 2017

1 Introduction

These notes develop the forward model for a wide class of single molecule fluorescence microscopes. We split the imaging process into four parts—illumination, excitation, emission, and detection—and analyze each part individually. For each part of the imaging process, we will perform a general analysis, relate the analysis to current techniques, and mention possible improvements.

1.1 Notation

We use boldface for vectors $\mathbf{r}$, hats for unit vectors $\hat{\mathbf{r}}$, normal face for vector lengths $r = |\mathbf{r}|$, tildes for matrices $\tilde{\mathbf{O}}$, and double arrows for tensors $\overleftrightarrow{\mathbf{G}}$.

1.2 Coordinates

First, we place the origin at the geometric focus of the microscope. If there are multiple objectives we assume that the foci are perfectly aligned. Next, we choose a fixed laboratory coordinate system using Cartesian unit vectors $\mathbf{r} = x\hat{\mathbf{x}} + y\hat{\mathbf{y}} + z\hat{\mathbf{z}}$.

2 Illumination

2.1 General Analysis

We view illumination as the process of establishing an electric field distribution $\mathbf{E}(\mathbf{r}, t)$ near the origin. In these notes we will use the complex spatial electric field $\mathbf{E}(\mathbf{r})$ related to the time dependent electric field by

$$\mathbf{E}(\mathbf{r}, t) = \mathrm{Re}\{\mathbf{E}(\mathbf{r})e^{-j\omega t}\}.$$

We will refer to the complex spatial electric field as the electric field. Analysis of the illumination pattern consists of finding the input electric field $\mathbf{E}_{\mathrm{in}}(\mathbf{r})$ near the focal point.

2.2 Current Techniques

2.2.1 Laser Köhler Illumination

Laser Köhler illumination is accomplished by focusing a laser beam onto the center of the back focal plane of the objective as shown in Figure 2(a) of [1]. Under laser Köhler illumination a constant electric field is established in the focal region. That is

$$\mathbf{E}_{\mathrm{in}}(\mathbf{r}) = \mathbf{P}$$

where $\mathbf{P}$ is the 3D vector pointing along the polarization direction of the laser. Under laser Köhler illumination the electric field in the focal region is always transverse, and the electric field is constant throughout the field of view.

If we use a modulated polarizing element on the illumination side, its pass direction will change $\mathbf{P}$.

Notice that both $\mathbf{E}$ and $\mathbf{P}$ are 3D vectors, not 2D Jones vectors. We will continue using 3D vectors throughout these notes so that we can consider illumination patterns from any angle.

2.2.2 Laser Critical Illumination

Laser critical illumination is accomplished by illuminating the entire back focal plane of the objective with a laser as shown in shown in Figure 2b) of [1]. Under laser critical illumination, the electric field varies near the focal plane. The electric field at every point can be calculated using the Richards-Wolf diffraction integral [2]. To calculate the electric field at a point we calculate the electric field at that point due to a single point on the lens, then integrate the contributions from each point while keeping track of the phase to allow for interference. See Chapter 3 of [3] for a complete calculation of the focal fields created by a spherical lens including consideration of under filling the back aperture and higher order laser modes.

If the back aperture receives uniform illumination, then the electric fields in the focal plane will be transverse and the electric fields away from the focal plane will have a transverse component. See Figures 8-10 of [4] for images of the fields.

Laser critical illumination only creates an appreciable electric field near the focal spot, so an image must be built up by scanning.

We can also illuminate the sample with a cylindrical lens. The electric field pattern created by a cylindrical lens can be found in [4].

Under laser critical illumination the electric field near the focal plane can be modified by modulating the intensity and phase in the back focal plane. Axial patterning, radial patterning, and "bone" patterning are some modulation patterns that have been explored [5].

2.3 Possible Techniques

2.3.1 Lamp Illumination

Lamp illumination could be used to provide inexpensive and novel illumination patterns. Under laser illumination we can establish a fixed electric field distribution, but under lamp illumination we need to consider the electric field at each point as a vector stochastic process. Analyzing the vector stochastic process requires a statistical optics approach that includes polarization effects.

The complete theory of coherence and polarization was completed in 2003 [6], and has not, to my knowledge, been applied to single molecule microscopy problems.

3 Excitation

3.1 General Analysis

Consider a two-level quantum system in the dipole approximation—an excellent model for many fluorophores. Each transition can be described by a *transition dipole moment*, a vector that points in a fixed direction with respect to the molecule's molecular structure. We denote the absorption dipole moment by $\boldsymbol{\mu}_{\text{abs}}$ (called $\boldsymbol{\mu}_{21}$ in quantum mechanics) and the emission dipole moment by $\boldsymbol{\mu}_{\text{em}}$ ($\boldsymbol{\mu}_{12}$). The transition dipole moments can be calculated analytically for simple systems using quantum mechanics, calculated numerically for complex systems using Hartree-Fock theory or density functional theory, or measured experimentally.

When a fluorophore with transition dipole moments $\boldsymbol{\mu}_{\text{em}}$ and $\boldsymbol{\mu}_{\text{abs}}$ is exposed to a weak electric field $\mathbf{E}$ that is constant near the fluorophore, the electric field creates an *induced dipole moment* $\boldsymbol{\mu}$ where

$$\boldsymbol{\mu} \propto \boldsymbol{\mu}_{\text{em}} \boldsymbol{\mu}_{\text{abs}}^{\dagger} \mathbf{E}_{\text{in}}.$$

The relationship between the incident electric field and the induced dipole moment is summarized by the

polarizability tensor $\overleftrightarrow{\boldsymbol{\alpha}}$ where

$$\boldsymbol{\mu} = \overleftrightarrow{\boldsymbol{\alpha}}\mathbf{E}_{\text{in}}$$
$$\overleftrightarrow{\boldsymbol{\alpha}} \propto \boldsymbol{\mu}_{\text{em}}\boldsymbol{\mu}_{\text{abs}}^{\dagger}$$

If we assume $\boldsymbol{\mu}_{\text{em}} = \boldsymbol{\mu}_{\text{abs}}$ then the induced dipole can only be created along a single axis relative to the molecule's structure. This assumption is invalid for many fluorophores—even GFP's transition dipole moments are a few degrees apart [7]. Some crystals have excitation and emission transition dipole moments that are orthogonal [8]!

General reference for this section: Appendix A of [3].

3.2 Current Techniques

Many single molecule orientation and location estimation experiments make the unstated assumption that $\boldsymbol{\mu}_{\text{em}} = \boldsymbol{\mu}_{\text{abs}}$. Under this assumption, the induced dipole direction is identical to the directions of the transition dipole moments.

Many groups approach the excitation analysis from a "power absorbed" or a "probability" viewpoint. In the their 2014 review [9], the Moerner group says that "the probability of absorption is proportional to $|\boldsymbol{\mu}_{\text{abs}} \cdot \mathbf{E}|^2$". This approach is identical to the induced dipole approach above. We deal with classical electric fields and induced dipole moments, while they deal with probabilities of photon absorption. We will take the modulus squared of the electric field during detection, so the approaches are identical.

3.3 Possible Techniques

3.3.1 Estimating The Induced Dipole Moment

With the analysis above, we can attempt to estimate the complete induced dipole moment, not just the orientation of the induced dipole moment.

3.3.2 Simultaneous Analysis of Illumination and Detection

Estimating the induced dipole moment allows us to simultaneously analyze the illumination and detection paths. To my knowledge, the illumination and detection paths have only been considered individually. A simultaneous analysis could allow us to find unique ways of modulating the illumination and detection paths together.

3.3.3 Estimating Both Transition Dipole Moments

If $\boldsymbol{\mu}_{\text{em}} \neq \boldsymbol{\mu}_{\text{abs}}$, then we may find techniques for simultaneously measuring both $\boldsymbol{\mu}_{\text{em}}$ and $\boldsymbol{\mu}_{\text{abs}}$. Measured both transition dipole moments could be useful for characterizing fluorophore and for measuring the effects of an environment on a fluorophore.

4 Emission

4.1 General Analysis

Consider an induced dipole moment $\boldsymbol{\mu}$ at $\mathbf{r}'$ in a medium with index of refraction n_1 with an as shown in Figure 1. The electric field distribution $\mathbf{E}_{\text{obj}}(\mathbf{r})$ is related to $\mathbf{r}'$ and $\boldsymbol{\mu}$ by the Green's tensor [3]

$$\mathbf{E}_{\text{obj}}(\mathbf{r}) = \overleftrightarrow{\mathbf{G}}(\mathbf{r}, \mathbf{r}')\boldsymbol{\mu} \tag{1}$$
$$\overleftrightarrow{\mathbf{G}}(\mathbf{r}, \mathbf{r}') = \left[\overleftrightarrow{\mathbf{I}} + \frac{1}{k^2}\nabla\nabla\right]\frac{e^{ikn_1R}}{4\pi R}. \tag{2}$$

Notice that $\mathbf{E}_{\text{obj}}$ and $\mathbf{E}_{\text{in}}$ are field with different frequencies, so they effectively don't interfere.

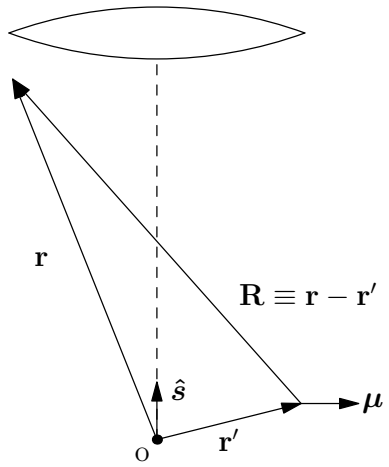

Figure 1: Position and orientation vectors.

After evaluating the gradients and only keeping the terms that persist in the far field ($R \gg \lambda$), the Green's tensor becomes

$$\overleftrightarrow{\mathbf{G}}_{FF}(\mathbf{r},\mathbf{r}') = \left[\overleftrightarrow{\mathbf{I}} - \frac{\mathbf{R}\mathbf{R}^{\dagger}}{R^2}\right]\frac{e^{ikn_1R}}{4\pi R}. \tag{3}$$

When the dipole is near the origin and we are considering the electric fields at points far from the origin ($r \gg r'$), we can use the approximations $\mathbf{R} \approx \mathbf{r}$ and $R \approx r - \mathbf{r}' \cdot \hat{\mathbf{r}}$. Using these approximations in Equation 3 with $R = r - \mathbf{r}' \cdot \hat{\mathbf{r}}$ in the phase term and $R = r$ everywhere else gives

$$\overleftrightarrow{\mathbf{G}}_{FF}(\mathbf{r},\mathbf{r}') = \left[\overleftrightarrow{\mathbf{I}} - \hat{\mathbf{r}}\hat{\mathbf{r}}^{\dagger}\right]\frac{e^{ikn_1(r-\mathbf{r}'\cdot\hat{\mathbf{r}})}}{4\pi r}. \tag{4}$$

4.1.1 Aside: Interpreting The Green's Tensor

The Green's tensor acts on a vector (the dipole moment) and outputs a vector field (the electric field). When we choose a particular point (say $r = 1$, $\theta_z = 0$, $\phi_{xy} = 0$), then the Green's tensor becomes a matrix and we can find the electric field at that point by matrix multiplication.

Alternatively, the Green's tensor can be interpreted as a mathematical shorthand for the $\mathbf{r} \times \boldsymbol{\mu} \times \mathbf{r}$ method [10] of calculating the fields created by a dipole moment.

4.2 Current Techniques

Compare equation 4 with equations 7 and 9 in [9]. While they consider a dipole at the origin and multiply by a phase term to consider defocus, the formulation above considers a dipole at an arbitrary location with respect to the origin. This generalization allows us to consider localizing the dipole from orthogonal views.

Notice that equation 4 can be evaluated using any convenient coordinate system. For example, if we express $\mathbf{r}$ in spherical coordinates [$\mathbf{r} = r\cos(\phi)\sin(\theta)\hat{\mathbf{x}} + r\sin(\phi)\sin(\theta)\hat{\mathbf{y}} + r\cos(\theta)\hat{\mathbf{z}}$] and $\mathbf{r}'$ in Cartesian coordinates [$\mathbf{r}' = x'\hat{\mathbf{x}} + y'\hat{\mathbf{y}} + z'\hat{\mathbf{z}}$] then:

$$\overleftrightarrow{\mathbf{G}}_{FF}(\mathbf{r},\mathbf{r}') = \begin{bmatrix} 1-\cos^2(\phi)\sin^2(\theta) & -\cos(\phi)\sin(\phi)\sin^2(\theta) & -\cos(\phi)\cos(\theta)\sin(\theta) \\ -\cos(\phi)\sin(\phi)\sin^2(\theta) & 1-\sin^2(\phi)\sin^2(\theta) & -\sin(\phi)\cos(\theta)\sin(\theta) \\ -\cos(\phi)\cos(\theta)\sin(\theta) & -\sin(\phi)\cos(\theta)\sin(\theta) & 1-\cos^2(\theta) \end{bmatrix}\frac{\Pi(\mathbf{r},\mathbf{r}')}{4\pi r} \tag{5}$$

$$\Pi(\mathbf{r},\mathbf{r}') = \exp\left[ikn_1(r - \{x'\sin(\theta)\cos(\phi) + y'\sin(\theta)\sin(\phi) + z'\cos(\theta)\})\right] \tag{6}$$

Compare equation 6 with equation 3 in [11]. We have derived the same phase expression except we don't ignore the e^{ikn_1r} term, and we correct the sign errors on the x' and y' terms.

4.3 Possible Techniques

4.3.1 Consideration of Dipoles At Any Position

The general analysis allows us to consider an induced dipole at any position. Existing analyses only consider dipoles along the optic axis [9].

5 Detection

5.1 General Analysis

5.1.1 Coordinates

When we are analyzing a microscope with a single optic axis, we typically choose $\hat{\mathbf{z}}$ parallel to the optic axis and define cylindrical and spherical coordinates with respect to $\hat{\mathbf{z}}$. In these notes, we want to consider arbitrary optic axes, so we will define spherical and cylindrical coordinates with respect to the optic axis.

To specify a set of spherical coordinates called the $\hat{\mathbf{s}}\hat{\mathbf{a}}$ spherical coordinates, we choose a zenith unit vector $\hat{\mathbf{s}}$ along the optic axis and an orthogonal unit vector $\hat{\mathbf{a}}$ then parameterize any vector $\mathbf{r}$ using the length of the vector (r), the angle between $\hat{\mathbf{s}}$ and $\mathbf{r}$ ($\theta_{\hat{\mathbf{s}}}$), and the angle between $\hat{\mathbf{a}}$ and the projection of $\mathbf{r}$ into the plane spanned by $\hat{\mathbf{a}}$ and $\hat{\mathbf{s}} \times \hat{\mathbf{a}}$ in the right-handed $\hat{\mathbf{s}}$ direction ($\phi_{\hat{\mathbf{a}},\hat{\mathbf{s}}\times\hat{\mathbf{a}}}$). For example, the $\hat{\mathbf{z}}\hat{\mathbf{x}}$ and $\hat{\mathbf{x}}\hat{\mathbf{y}}$ spherical coordinates are shown in Figures 2(a) and 2(b).

Similarly, to specify a set of cylindrical coordinates called the $\hat{\mathbf{s}}\hat{\mathbf{a}}$ cylindrical coordinates, we choose a zenith unit vector $\hat{\mathbf{s}}$ along the optic axis and an orthogonal unit vector $\hat{\mathbf{a}}$ then parameterize any vector $\mathbf{r}$ using the length of the vector projected into the $\hat{\mathbf{s}}$ direction ($s_{\hat{\mathbf{s}}}$), the length of the vector projected into the plane spanned by $\hat{\mathbf{a}}$ and $\hat{\mathbf{s}} \times \hat{\mathbf{a}}$ ($\rho_{\hat{\mathbf{a}},\hat{\mathbf{s}}\times\hat{\mathbf{a}}}$), and the angle between $\hat{\mathbf{a}}$ and the projection of $\mathbf{r}$ into the plane spanned by $\hat{\mathbf{a}}$ and $\hat{\mathbf{s}} \times \hat{\mathbf{a}}$ in the right-handed $\hat{\mathbf{s}}$ direction ($\phi_{\hat{\mathbf{a}},\hat{\mathbf{s}}\times\hat{\mathbf{a}}}$). For example, the $\hat{\mathbf{z}}\hat{\mathbf{x}}$ and $\hat{\mathbf{x}}\hat{\mathbf{y}}$ spherical coordinates are shown in Figures 2(c) and 2(d).

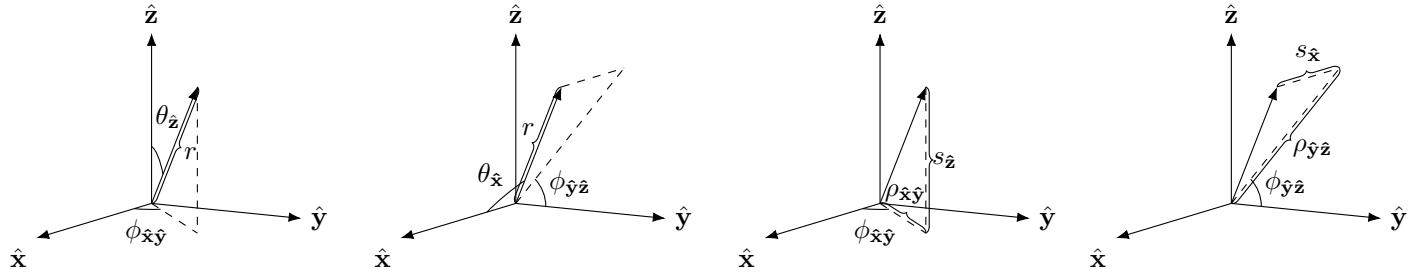

(a) $\hat{\mathbf{z}}\hat{\mathbf{x}}$ spherical coordinates. (b) $\hat{\mathbf{x}}\hat{\mathbf{y}}$ spherical coordinates. (c) $\hat{\mathbf{z}}\hat{\mathbf{x}}$ cylindrical coordinates. (d) $\hat{\mathbf{x}}\hat{\mathbf{y}}$ cylindrical coordinates.

Figure 2: Coordinate systems.

5.1.2 Electric Field In The Back Focal Plane

We can model the action of the objective on the electric fields by a position dependent rotation matrix.

A right handed rotation about a vector $\hat{\mathbf{u}} = u_x\hat{\mathbf{x}} + u_y\hat{\mathbf{y}} + u_z\hat{\mathbf{z}}$ by angle θ can be represented by the rotation matrix

$$\tilde{\mathbf{R}}_{\hat{\mathbf{u}}}(\theta) = \begin{bmatrix} \cos\theta + u_x^2(1-\cos\theta) & u_x u_y(1-\cos\theta) - u_z\sin\theta & u_x u_z(1-\cos\theta) + u_y\sin\theta \\ u_y u_x(1-\cos\theta) + u_z\sin\theta & \cos\theta + u_y^2(1-\cos\theta) & u_y u_z(1-\cos\theta) - u_x\sin\theta \\ u_z u_x(1-\cos\theta) - u_y\sin\theta & u_z u_y(1-\cos\theta) + u_x\sin\theta & \cos\theta + u_z^2(1-\cos\theta) \end{bmatrix} \tag{7}$$

$$\tilde{\mathbf{R}}_{\hat{\mathbf{u}}}(\theta) = \cos\theta\tilde{\mathbf{I}} + \sin\theta\,[\hat{\mathbf{u}}]_\times + (1-\cos\theta)\hat{\mathbf{u}}\hat{\mathbf{u}}^\dagger \tag{8}$$

where $[\hat{\mathbf{u}}]_\times$ is the cross product matrix of $\hat{\mathbf{u}}$ [12].

A lens rotates electric fields into the plane perpendicular to the optic axis (equivalently, a lens rotates each ray parallel to the optic axis). The rotation matrix that describes the rotation of the electric field at $\hat{\mathbf{r}}$ by a lens with optic axis $\hat{\mathbf{s}}$ is

$$\tilde{\mathbf{R}}_{\hat{\mathbf{r}}\times\hat{\mathbf{s}}}(\text{acos}(\hat{\mathbf{r}}\cdot\hat{\mathbf{s}})) = (\hat{\mathbf{r}}\cdot\hat{\mathbf{s}})\tilde{\mathbf{I}} + \sqrt{1-(\hat{\mathbf{r}}\cdot\hat{\mathbf{s}})^2}\,[\hat{\mathbf{r}}\times\hat{\mathbf{s}}]_\times + (1-\hat{\mathbf{r}}\cdot\hat{\mathbf{s}})(\hat{\mathbf{r}}\times\hat{\mathbf{s}})(\hat{\mathbf{r}}\times\hat{\mathbf{s}})^\dagger \tag{9}$$

To conserve energy, we need to multiply the rotation matrix by a factor of $\sqrt{\frac{n_1}{n_0(\hat{\mathbf{r}}\cdot\hat{\mathbf{s}})}}$ [3] where n_0 is the index of refraction of the lens. Finally, we truncate the electric fields to simulate the finite numerical aperture of the lens. The final matrix that represents the lens is given by

$$\tilde{\mathbf{O}}_{\hat{\mathbf{s}}} = \sqrt{\frac{n_1}{n_o(\hat{\mathbf{r}}\cdot\hat{\mathbf{s}})}}\Pi\left(\frac{|\mathbf{r}-(\mathbf{r}\cdot\hat{\mathbf{s}})\hat{\mathbf{s}}|}{\rho_{\max}}\right)\tilde{\mathbf{R}}_{\hat{\mathbf{r}}\times\hat{\mathbf{s}}}(\text{acos}(\hat{\mathbf{r}}\cdot\hat{\mathbf{s}})) \tag{10}$$

where $|\mathbf{r}-(\mathbf{r}\cdot\hat{\mathbf{s}})\hat{\mathbf{s}}|$ is the shortest distance from r to the optic axis, $\rho_{\max}$ is the radius of the objective lens ($\rho_{\max} = f_{\text{obj}}\tan\left(\arcsin\left(\frac{\text{NA}}{n_1}\right)\right)$), and

$$\Pi(x) = \begin{cases} 1, |x| < 1 \\ 0, |x| > 1 \end{cases}. \tag{11}$$

Now that we can compute the effect of the objective lens, we can compute the electric field in the back focal plane

$$\mathbf{E}_{\text{bfp}} = \tilde{\mathbf{O}}_{\text{obj}}\overleftrightarrow{\mathbf{G}}_{FF}\boldsymbol{\mu} \tag{12}$$

If we place a polarizing element in the back focal plane, $\mathbf{E}_{\text{bfp}}$ will be projected onto the pass direction of the polarizing element.

The intensity in the back focal plane is given by

$$I_{\text{bfp}}(\mathbf{r}) = \mathbf{E}_{\text{bfp}}^\dagger\mathbf{E}_{\text{bfp}} = |\mathbf{E}_{\text{bfp}}|^2. \tag{13}$$

5.1.3 Electric Field In The Image Plane

If $f_{\text{obj}} \ll f_{\text{tube}}$, then the paraxial approximation applies and

$$\mathbf{E}_{\text{img}}(\mathbf{r}'') = \mathcal{F}_{3D}\{\mathbf{E}_{\text{bfp}}\}|_{\lambda f_{\text{tube}}} = \int_{\mathbb{R}^3}\mathbf{E}_{\text{bfp}}e^{-i\frac{k}{f_{\text{tube}}}\mathbf{r}\cdot\mathbf{r}''}d\mathbf{r}. \tag{14}$$

where $\mathbf{r}''$ is the position in the image plane. If we place a polarizing element in the imaging plane, $\mathbf{E}_{\text{img}}$ will be projected onto the pass direction of the polarizing element.

Finally, the intensity in the image plane is

$$I_{\text{img}}(\mathbf{r}'') = \mathbf{E}_{\text{img}}^\dagger\mathbf{E}_{\text{img}} = |\mathbf{E}_{\text{img}}|^2. \tag{15}$$

Notice that we take the 3D Fourier transform instead of the usual 2D. The objective lens rotates the electric fields to the transverse plane, so the usual 2D FT is equivalent to the 3D FT evaluated in any transverse plane. I've used the 3D FT to simplify the notation and show that we can use the same operation for any optic axis.

Also note that the Fourier transform is acting on a vector field instead of the usual scalar field. The FT of a vector field is just the usual scalar FT applied to each component of the vector.

5.2 Current Techniques

5.2.1 Single View

If the optic axis is along the $\hat{\mathbf{z}}$ axis and we have an infinite numerical aperture, the objective lens matrix reduces to

$$\tilde{\mathbf{O}}_{\hat{\mathbf{z}},\text{obj}} = \sqrt{\frac{n_1}{n_o \cos(\theta_z)}} \begin{bmatrix} \cos(\theta_z)\cos^2(\phi_{xy}) + \sin^2(\phi_{xy}) & (\cos(\theta_z) - 1)\sin(\phi_{xy})\cos(\phi_{xy}) & -\sin(\theta_z)\cos(\phi_{xy}) \\ (\cos(\theta_z) - 1)\sin(\phi_{xy})\cos(\phi_{xy}) & \cos(\theta_z)\sin^2(\phi_{xy}) + \cos^2(\phi_{xy}) & \sin(\theta_z)\sin(\phi_{xy}) \\ \sin(\theta_z)\cos(\phi_{xy}) & \sin(\theta_z)\sin(\phi_{xy}) & \cos(\theta_z) \end{bmatrix}. \tag{16}$$

Equation 16 is identical to equation 11 in [9] and equation 2 in Fourkas' paper [10]. Fourkas sums the intensity over the entire image plane, while we consider the complete imaging model. In our formulation, we combine the effects of NA, the apodization, and the rotation of the lens into a single matrix $\tilde{\mathbf{O}}$ (Equation 10).

5.2.2 Back Focal Plane Manipulation

The Moerner group has used a variety of phase and amplitude masks in the back focal plane of the detection path [9]. These techniques effectively change the point spread function of the detection system.

5.3 Possible Techniques

5.3.1 Arbitrary Views Of A Dipole Near The Focal Point

The work in the general analysis section allows us to calculate the images created by multiple views along arbitrary optic axes. This allows us to analyze new geometries like diSPIM.

6 Complete Forward Model

Combining all of the previous sections gives the complete forward model:

$$I_{\text{img}}(\mathbf{r}'') = \left| \mathcal{F}_{3D} \left\{ \tilde{\mathbf{O}}_{\text{obj}} \overleftrightarrow{\mathbf{G}}_{FF} \overleftrightarrow{\boldsymbol{\alpha}} \mathbf{E}_{\text{in}} \right\} \right|^2. \tag{17}$$

where

$\mathbf{E}_{\text{in}}$ is the incident electric field pattern established by the illumination optics. It is a function of the input light source, input light pattern (phase, amplitude, polarization modulation), and input light optics (spherical, cylindrical lens).

$\overleftrightarrow{\boldsymbol{\alpha}}$ is the polarizability tensor. It is a function of the fluorophore type and the fluorophore's orientation.

$\overleftrightarrow{\mathbf{G}}_{FF}$ is the Green's tensor that generates the electric fields far from the induced dipole moment. It is a function of the dipole moment's position and the refractive index of the medium.

$\tilde{\mathbf{O}}_{\text{obj}}$ is the matrix that describes the action of the objective lens. It is a function of the objective's focal length, NA, and optic axis.

References

[1] Mikael P. Backlund, Matthew D. Lew, Adam S. Backer, Steffen J. Sahl, and W. E. Moerner. The role of molecular dipole orientation in single-molecule fluorescence microscopy and implications for super-resolution imaging. *ChemPhysChem*, 15(4):587–599, 2014.

[2] B. Richards and E. Wolf. Electromagnetic diffraction in optical systems. ii. structure of the image field in an aplanatic system. *Proceedings of the Royal Society of London A: Mathematical, Physical and Engineering Sciences*, 253(1274):358–379, 1959.

[3] Lukas Novotny and Bert Hecht. *Principles of nano-optics*. Cambridge University Press, 2006.

[4] K. S. Youngworth and T. G Brown. Focusing of high numerical aperture cylindrical-vector beams. *Opt. Express*, 7(2):77–87, Jul 2000.

[5] A. Débarre, R. Jaffiol, C. Julien, D. Nutarelli, A. Richard, P. Tchénio, F. Chaput, and J.-P. Boilot. Quantitative determination of the 3d dipole orientation of single molecules. *The European Physical Journal D - Atomic, Molecular, Optical and Plasma Physics*, 28(1):67–77, 2004.

[6] Emil Wolf. Unified theory of coherence and polarization of random electromagnetic beams. *Physics Letters A*, 312(56):263 – 267, 2003.

[7] Federico I. Rosell and Steven G. Boxer. Polarized absorption spectra of green fluorescent protein single crystals: transition dipole moment directions. *Biochemistry*, 42(1):177–183, 2003. PMID: 12515552.

[8] Felix Koberling, Ute Kolb, Gnther Philipp, Inga Potapova, Thomas Basch, and Alf Mews. Fluorescence anisotropy and crystal structure of individual semiconductor nanocrystals. *The Journal of Physical Chemistry B*, 107(30):7463–7471, 2003.

[9] Adam S. Backer and W. E. Moerner. Extending single-molecule microscopy using optical fourier processing. *The Journal of Physical Chemistry B*, 118(28):8313–8329, 2014. PMID: 24745862.

[10] John T. Fourkas. Rapid determination of the three-dimensional orientation of single molecules. *Opt. Lett.*, 26(4):211–213, Feb 2001.

[11] Anurag Agrawal, Sean Quirin, Ginni Grover, and Rafael Piestun. Limits of 3D dipole localization and orientation estimation for single-molecule imaging: towards green's tensor engineering. *Opt. Express*, 20(24):26667–26680, Nov 2012.

[12] Rotation Matrix. `https://en.wikipedia.org/wiki/Rotation_matrix#Rotation_matrix_from_axis_and_angle`. [Online; accessed 30-January-2017].